Journal of Hydraulic Structures
J. Hydraul. Struct., 2020; 6(1): 1-19
DOI: 10.22055/jhs.2020.31418.1124

OPEN ACCESS

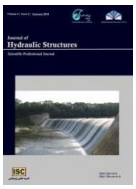

Investigation of concentration polarization in a cross-flow nanofiltration membrane: Experiment and CFD modelling

Hossein Asefi[1]
Abolghasem Alighardashi[2]
Mojtaba Fazeli[2]
Amir Fouladitajar[3]

Abstract

Numerous researches have been investigated on the mass transfer phenomena and hydrodynamics for the fluid in the vicinity of the membrane surface by the mathematical modelling and simulation. Due to complexities involved in solving transport phenomena within membranes, the application of CFD simulation study for determining the concentration polarization (CP) profile in the membrane channel is limited. In this study, a 2D CFD modelling and simulation of CP phenomena in nanofiltration of an aqueous solution of MgSO47H2O in a vertical spacer-filled flat sheet membrane module was presented. A response surface methodology (RSM) statistical analysis has been designed in order to fully capture effects of variations of the feed liquid flow and the transmembrane pressure (TMP) on the permeate flux and concentration. It was also shown that increasing TMP or the liquid flow rate led to enhancing the permeate flux while increasing the feed concentration decreased it. The simulated results were validated and compared with the available experimental data, showing a satisfactory agreement. Eventually, the mass transfer coefficient derived from CFD simulations and calculated from Sherwood empirical relationships were compared which showed 10% and 33% difference in lower and higher liquid flow rates, respectively.

Keywords: Concentration polarization; Nanofiltration; Sherwood number; Mass transfer coefficient; CFD modelling.

Received: 10 October 2019; Accepted: 1 January 2020

[1] Department of Civil, Water and Environmental Engineering, Shahid Beheshti University, Tehranpars, Tehran, Iran. h_asefi@sbu.ac.ir **.(Corresponding author)**
[2] Department of Civil, Water and Environmental Engineering, Shahid Beheshti University, Tehranpars, Tehran, Iran
[3] College of Petroleum and Chemical Engineering, Science and Research Branch, Islamic Azad University, Tehran, Iran.

1. Introduction

During the recent decades, various membrane techniques have raised in the treatment of saline water. Development of membrane technology has the potential to facilitate the drinking water supply. In this technology, the nature of semipermeable membranes is the main cause of separation. Accumulation of particles in the feed channel is known as the fouling phenomena which may fall into several categories including organic, colloidal, inorganic, and microbial fouling. Flux decline can be a possible result of the membrane fouling and concentration polarization (CP) phenomena [1–3] Researchers have shown that the CP caused a drop in the membrane performance up to 30% [4]. Various methods have been proposed for controlling the CP, two of which are declining the water flux (J) and increasing the mass transfer coefficient (K). A number of previous studies have also reported that increasing the liquid cross-flow velocity, improvement of hydrodynamic properties, and promoting turbulent flow can all help to disrupt the CP [5]. Generally, common methods applied in the literature for controlling the CP phenomena are unsteady state flow [6], flushing [7], gas/liquid two-phase unsteady flow [8–10], membrane vibration [11], and DC electric field [12].

During the past few decades, much research has been carried out with a focus on the CP phenomena both experimentally and numerically. CFD simulations developed the turbulent promoter research. It was therefore revealed that the turbulent promoter affected the wall shear stress, mass transfer coefficients, the dimensionless groups' plane (N's, Nf)), the permeate flux, the mass transfer boundary layer, and so on [9–22].

Schock and Miquel [15] investigated the pressure drop and the mass transfer coefficient in spacer filled and spacer free channels. They could design optimum of spiral wound element by a computer program. Sutzkover et al. [23] proposed a simple method for computing the mass transfer coefficient. Their technic assessed the Reynolds region of 1000 to 2600. Gekas and Hallstrom [16] studied the Sherwood equation, Schmidt and Reynolds numbers under turbulent flow situations. They discussed the effective factors due to the concentration gradient in RO and UF membranes. They also depicted regions of Re and Sc numbers for validity of the Sherwood equation. Geraldes and Afonso [24] performed a CFD simulation to estimate the correct factor for the convective mass transfer coefficient under laminar flow in NF and RO membranes. Then, Fernández-Sempere et al. [25] measured the thickness of the CP layer on RO membranes by Digital Holographic Interferometry (DHI). Then, the results were compared with the modified convective mass transfer coefficient measured by Geraldes and Afonso. They showed that the results were close at turbulent flow.

Wardeh and Morvan [22] simulated the CP phenomena and effects of zigzagging and submerged spacers using ANSYS-CFX software. They proved that zigzagging spacers are more desirable in comparison with the submerged spacer. Subramani et al [26] et al. assessed the CP layer in open and spacer filled membrane channels with the aid of the film theory, finite element and finite difference methods. They simulated an impermeable wall, one permeable wall and two permeable walls in the channel by the finite element method, and then compared the results. Despite the previous reports, it was shown that the cavity and submerged spacer could improve the mass transfer more than zigzagging spacers. It was revealed that the stagnant region in front of and behind the spacer filaments increased the CP layer. Geraldes et al. [27] compared the filaments adjacent to the membrane with filaments adjacent to the wall. They proved that presence of the spacers increases the shear stress, but the CP was controlled in the presence of filaments adjacent to the membrane. It was also shown that the filaments adjacent to the membrane could decrease the CP up to 50%. Salcedo-Díaz et al. [28] measured the thickness of

the CP layer in length and height of the slit feed channel by Digital Holographic Interferometry (DHI) technic revealing that the concentration of the CP layer in the middle of the feed channel gets maximum. Ahmad and Lau [29] carried out a CFD study for unsteady state flow in a spacer filled channel using FLUENT-6 software proving that spherical spacers decrease the CP layer more than cube spacers. Li et al. [17] performed a 3-D CFD analysis to evaluate the CP phenomena in the RO feed channel showing profiles of the local mass transfer coefficient in spacer-filled and spacer free channels using four different velocities. It was demonstrated that spacers increase both the pressure drop and the velocity on the membrane surface. Furthermore, filaments form concentrates rolling cells at the center of the feed channel. Kim and Hoek [30] compared analytical CP models with a more rigorous numerical CP model and experimental CP data. All experiments were performed considering the NaCl solution as the feed on the RO membrane. It was proved in this work that results from the film theory and the numerical model were in an acceptable agreement.

The concentration polarization is a complex phenomenon which has been a challenge for researchers. Prediction of this phenomenon helps one to optimize the separation process. In this study, a vertical flat sheet membrane is simulated by solving the 2D unsteady governing equations in a spacer-filled empty channel. CFD results were then validated with the available experimental data. Effects of the feed concentration, the liquid flow and the TMP on the permeate flux and concentration were studied by RSM analysis.

2. Materials and methods

2.1. Preparation of feed

An aqueous solution of MgSO47H2O (Merck, Germany) with the concentration of 250 mg/l to 4750 mg/l was used. For preparation of aqueous solutions, deionized water ($EC < 1\ \mu S/cm$) was used. The temperature of the aqueous solution was adjusted at 25+0.5 ℃. Volume of the solution tank was 25 liters. Water conductivity in the feed and the permeate solution was measured by WTW (Germany). Osmotic pressure, density, and diffusion coefficient were calculated from the following formulas [31]:

$$\pi(\text{bar}) = 4.97\text{m}_\text{A}(49.55 - 136.7\text{m}_\text{A} + 1207{\text{m}_\text{A}}^2) \quad (1)$$

$$\text{Density, } \rho\ \left(\frac{\text{kg}}{\text{m3}}\right) = 997 + 1036\text{m}_\text{A} \quad (2)$$

$$\text{Viscosity, } \mu\ (\times 10^{-3}\ \text{Pa s}) = 0.897(1 + 3.713\text{m}_\text{A} + 26.0614{\text{m}_\text{A}}^2) \quad (3)$$

$$\text{Diffusion coefficient, DAB } \left(\times 10^{-9}\frac{\text{m2}}{\text{s}}\right) = 0.849(1 - 0.41873{\text{m}_\text{AW}}^{0.0872}) \text{ for } \text{m}_\text{A} < 0.06 \quad (4)$$

m_A is solute mass fraction (kg solute/kg solution, m_Aw is solute mass fraction on membrane surface (kg solute/kg solution), π is osmotic pressure (Pa).

2.2. Filtration module

NF-2 membrane was used from SEPRO membrane (USA). Thickness of polyamide NF-2 membrane, pore size (pore radius), and porosity were set as 160 μm, 0.392 μm, and 0.467%, respectively. A flat sheet module was designed and fabricated from Plexiglas. This module was

made up of two plates with slit channel dimensions of 0.3×5×10 cm^3 as height, width, and length of the rectangle for inlet feed (Fig. 1). Spacer filaments were also used in a submerged configuration (as shown in Fig. 3). The membrane sheet was fixed in the feed channel with active area of 5×10 cm^2. More details about the module can be found in [8,18]. Filtration module was oriented vertically for all experiments.

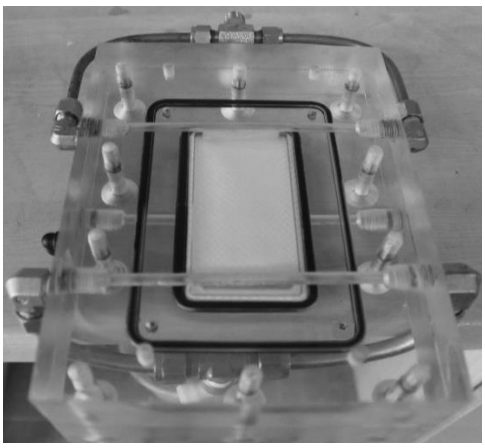

Figure 1. The experimental flat sheet module

2.3. Experimental setup

Fig. 2 demonstrates the schematic diagram of the experimental setup. A 25 L feed tank was used to keep the brackish water which was delivered to the membrane module by a centrifugal recirculation pump controlled by an inverter. This pump also supplied the required constant operating pressure to the feed. Two needle valves were placed on the feed and retentate lines so as to adjust the stream flow rate. Moreover, the valve was installed after the membrane module could apply a backpressure along the membrane unit. Pressure gauges (Wika, Germany, Accuracy is 0.1 bar) were employed before and after the membrane module to observe the inlet feed pressure. Details of the apparatus can be found in a previous publication [18].

2.4. Experimental procedures

As the first step, the distilled water permeate was measured in different feed pressures to compute the permeability of the membrane. The permeability, L_P, is 17.2 $L/(m^2.h.bar)$. In the second step, the experiments were designed by Design-Expert software (version 7.0.0). All experiments were repeated twice (Table 2). A new membrane was used for each test. The average duration of each experiment was 4 hours. The feed solution was injected to the vertical membrane flat sheet by means of a high-pressure pump. The permeate water was measured by a digital balancer (AND GF600-Japan, Accuracy is 0.001 g) connected to a PC computer recording data every ten seconds. In order for the feed properties not to change, the retentate was cycled to the feed tank.

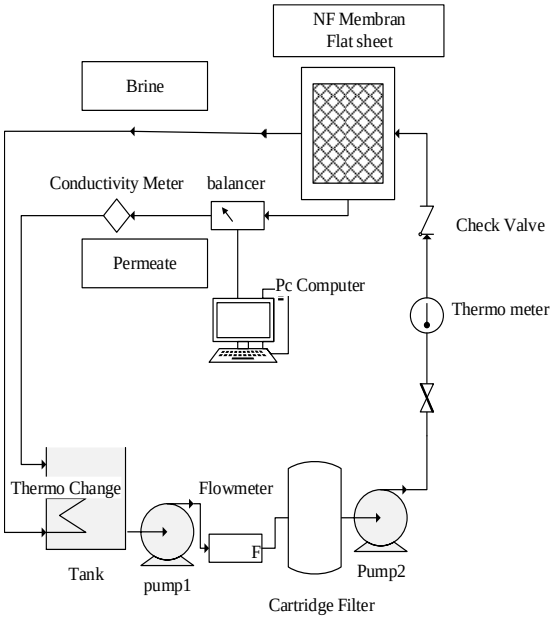

Figure 2. Schematic flow diagram of the experimental setup.

2.5. Experimental design

Response surface methodology (RSM) is a modern method for designing and analysis of experiments. This method is used for investigating multiple factor effects using several levels. RSM was used for optimization of modified NF and RO membranes [32,33]. In this work, a three-level-factor central composite design (CCD) was used to evaluate the influence of operation conditions on the permeate flux and the permeate electro conductivity. Three factors, namely feed concentration (mg/l), TMP (bar) and liquid velocity (m/s), were considered (Table 1). Therefore, a set of experiments was designed. Totally, 19 experiments were performed (Table 2).

Table 1. The experimental parameters and levels

Parameters	Feed concentration (mg/l)	TMP (bar)	Liquid velocity (m/s)
Levels	1000	6	0.22
	2000	9	0.44
	4000	12	0.66

Table 2. Experimental runs

Run	Factor 1 A:P Bar	Factor 2 B:Q l/min	Factor 3 C:C Ppm
1	12	2	4000
2	6	2	4000
3	9	4	2500
4	9	4	2500
5	6	2	1000
6	12	6	1000
7	6	6	1000
8	9	4	2500
9	9	1	2500
10	12	2	1000
11	12	6	4000
12	13.5	4	2500
13	9	4	2500
14	9	4	250
15	4.5	4	2500
16	9	4	2500
17	9	4	4750
18	9	7	2500
19	6	6	4000

3. Theory

3.1. Geometry reconstruction

The CFD simulations were primarily conducted to determine CP in spacer-filled channel of NF membranes. Dimensions of the feed channel were mentioned in the previous section. According to geometry of the slit channel, the height to width ratio was far less than unity (h/w=0.06). Therefore, the effect of side flow and walls were neglected. Then, the model was simulated to be 2D for CFD calculations. A mesh independence study was also carried out to eliminate the effect of mesh quality and size on the simulation results. To do so, simulation results were inspected using different mesh resolutions in order to find the optimal element size on the condition that the influence of the finer mesh is not larger than 2%. Thus, a mesh independence study was carried out considering TMP, feed concentration, and inlet velocity of 6 bar, 1000 mg/l, and 2 m/s, respectively. As Fig. 4 shows, the maximum CP changes only about 2% by refining the element size from 28866 to 205150 whereas the corresponding computational time increases dramatically. Therefore, resolution of the medium element size seems acceptable

to guarantee the accuracy of simulations. Finally, it was proved that the optimal mesh statistics was 47000 quadrilateral elements considering adequate mesh inflation around the spacers. All grid sizes were in the range of 0.01 to 2 mm. The dimensions were measured carefully from the experimental set-up using a Vernier Caliper with 0.01 mm accuracy.

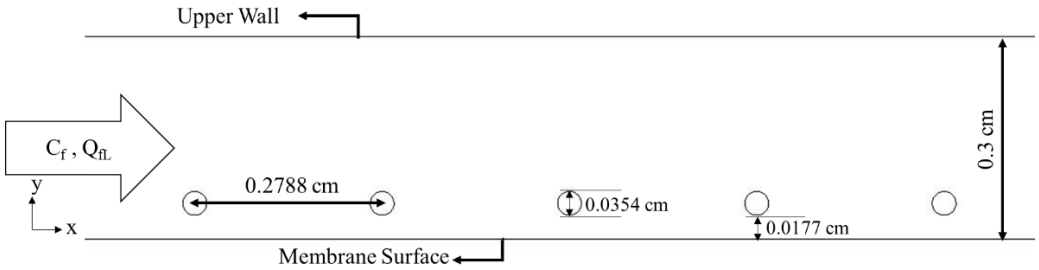

Figure 3. 2D schematic view of the computational domain.

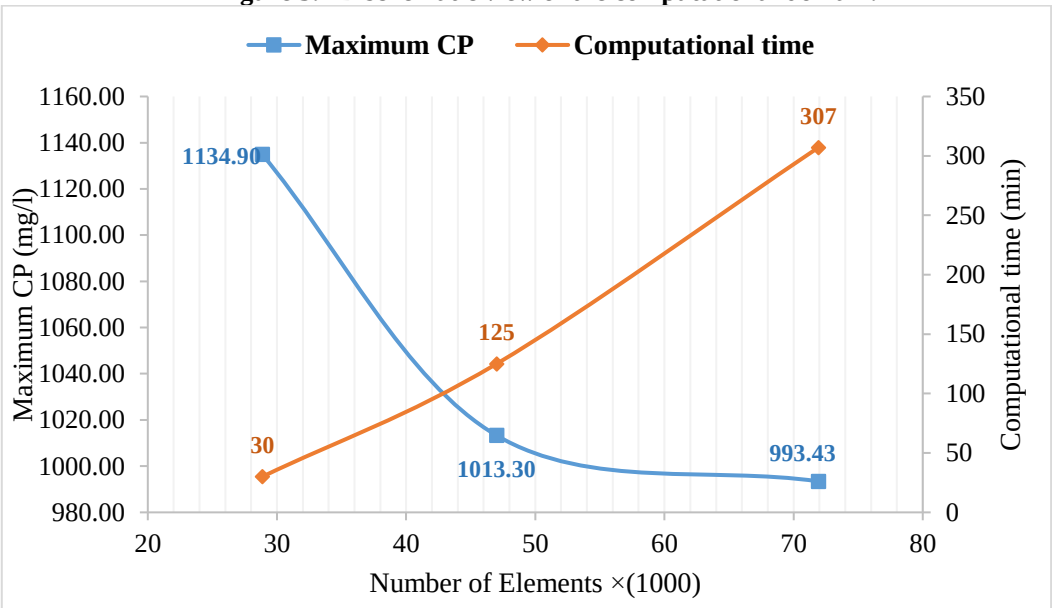

Figure 4. Mesh independence study (maximum CP (mg/l) and computational time of simulations (min) vs. number of elements).

3.2. Analytical film theory model

The film theory approach simplifies a complex transport problem. In this theory, the axial solute convection on the membrane surface vicinity was ignored and a fully developed boundary layer was assumed. Therefore, the mass transfer problem was considered one-dimensional. The convection-diffusion mass balance from the membrane surface out to the film layer gave the relationship between the permeate flux and CP, expressed as:

$$\frac{m_{AW} - m_{AP}}{m_{A0} - m_{AP}} = \exp\left(\frac{J}{K}\right) \quad (5)$$

where k, m_{A0}, m_{AP}, and J are the mass transfer coefficient, bulk solute concentration, permeate

solute concentration, and permeate water flux through the membrane, respectively. The mass transfer coefficient greatly depends on the flow hydrodynamics estimated by the following empirical relationship [2]:

$$K = \frac{D}{\delta} \tag{6}$$

where D and δ are the solute diffusion coefficient and film layer thickness, respectively. The mass transfer coefficient (k) can be related to the Sherwood number (Sh) adopting the following empirical equation derived for laminar flow [34]:

$$Sh = \frac{kd_h}{D} = 1.62(\frac{d_h u}{v})^{\frac{1}{3}}(\frac{\vartheta}{D})^{\frac{1}{3}}(\frac{d_h}{L})^{\frac{1}{3}} \tag{7}$$

where d_h is the hydraulic diameter, u is the flow velocity, ϑ is the kinematic viscosity, D is the solute diffusivity in water, and L is the length of the membrane channel.

3.3. Governing equation

In this work, the solution of $MgSO_4 7H_2O$ salt and deionized water was assumed to be isothermal and incompressible. Calculations were carried out for unsteady state laminar flow conditions of an open channel (Re=371-2600). The permeate velocity was small enough to ignore effects of the permeate velocity on the surface velocity [30]. The flow hydrodynamic and concentration polarization phenomena were analyzed by the Eulerian based solution of continuity, Navier–Stokes and Solute conservation equations [35]. Water was considered as the continuous fluid while salt was set as the dispersed phase.

$$\frac{\partial}{\partial t}(\alpha_k \rho_k) + \nabla.(\alpha_k \rho_k u_k) = 0 \tag{8}$$

α_k, ρ_k, and u_k are volume fraction, density and velocity vector of phase k.
Navier–Stokes equation:

$$\frac{\partial}{\partial t}(\alpha_k \rho_k u_k) + \nabla.(\alpha_k \rho_k u_k u_k) = \nabla.(\alpha_k \mu_k(\nabla u_k + (\nabla u_k)^T)) - \alpha_k \nabla p + \alpha_k \rho_k \boldsymbol{g} + \boldsymbol{M}_k \tag{9}$$

where p is the pressure field and μ_k is the viscosity of phase k. $\boldsymbol{M}_k$ is the interfacial momentum source term that shows interfacial forces on phase k due to the presence of the other phase and obeys the following condition:

$$\sum_{k=1}^{2} \boldsymbol{M}_k = \boldsymbol{M}_m \tag{10}$$

Solute conservation equation:

$$\frac{\partial c}{\partial t} + u\frac{\partial c}{\partial x} + v\frac{\partial c}{\partial y} = D(\frac{\partial^2 c}{\partial x^2} + \frac{\partial^2 c}{\partial y^2}) \tag{11}$$

where c is the salt concentration.
The above differential equations were solved using the following set of boundary conditions.

- Dirichlet boundaries were implemented for the inlet of the feed channel with prescribed velocity and salt concentration:

x=0, 0<y<h (h =0.3 cm)
$u_l = u_{l0}, v_l = 0,\ m_A = m_{A0}$ (12)

- Zero gradient boundary conditions were set for all dependent variables at the channel outlet:

x=L, 0<y<h (L =10 cm)
$\frac{\partial u_l}{\partial x} = 0 \quad , \quad \frac{\partial v_l}{\partial x} = 0 \quad , \quad \frac{\partial m_A}{\partial x} = 0$ (13)

- No-slip, no-penetration boundary conditions were considered for the upper wall as well as spacers:

0<x<L, y=h
$u_l = 0, v_l = 0, D\frac{\partial c}{\partial n} = 0$ (14)

- The following coupled equations were imposed for the velocity and salt concentration at the membrane surface:

0<x<L, y=0
$v = J_v = L_p\{\Delta P - \sigma[\pi(m_{AW}) - \pi(Rm_{AW})]\}, u = 0$ (15)

$D\frac{\partial c}{\partial n} = J_v(c_{Aw} - c_{Ap})$ (16)

A finite volume analysis was implemented to solve the aforementioned equations. In this work, the well-known PISO (Pressure-Implicit with Splitting of Operators) algorithm was implemented [36]. Besides, PRESTO (PREssure Staggering Option) and QUICK (Quadratic Upstream Interpolation for Convective Kinetics) were also adopted to enhance the level of accuracy. Simulations typically took two hours using Intel® Core™ i5-3317U 1.70 GHz CPU and 8 GB of RAM.

4. Result and discussion

4.1. Permeate concentration and flux

CFD simulation and experimental results of the permeate concentration and the permeate flux are depicted in Fig. 5. A comparison shows that there is a good agreement between CFD and experimental results with maximum and minimum errors of 10.5% and 0.166%, respectively. It should also be noted that the small difference between experimental and CFD results in this part is due to calibration of CFD data to resemble the experiments. In other words, the permeate flux

and concentration were allowed to change values in a broad range (between 0 and 300 L m-2 h-1) using the optimization tools to find the nearest value to that of experiments. Then, it can be guaranteed that the CP phenomenon predicted by the CFD is close to reality.

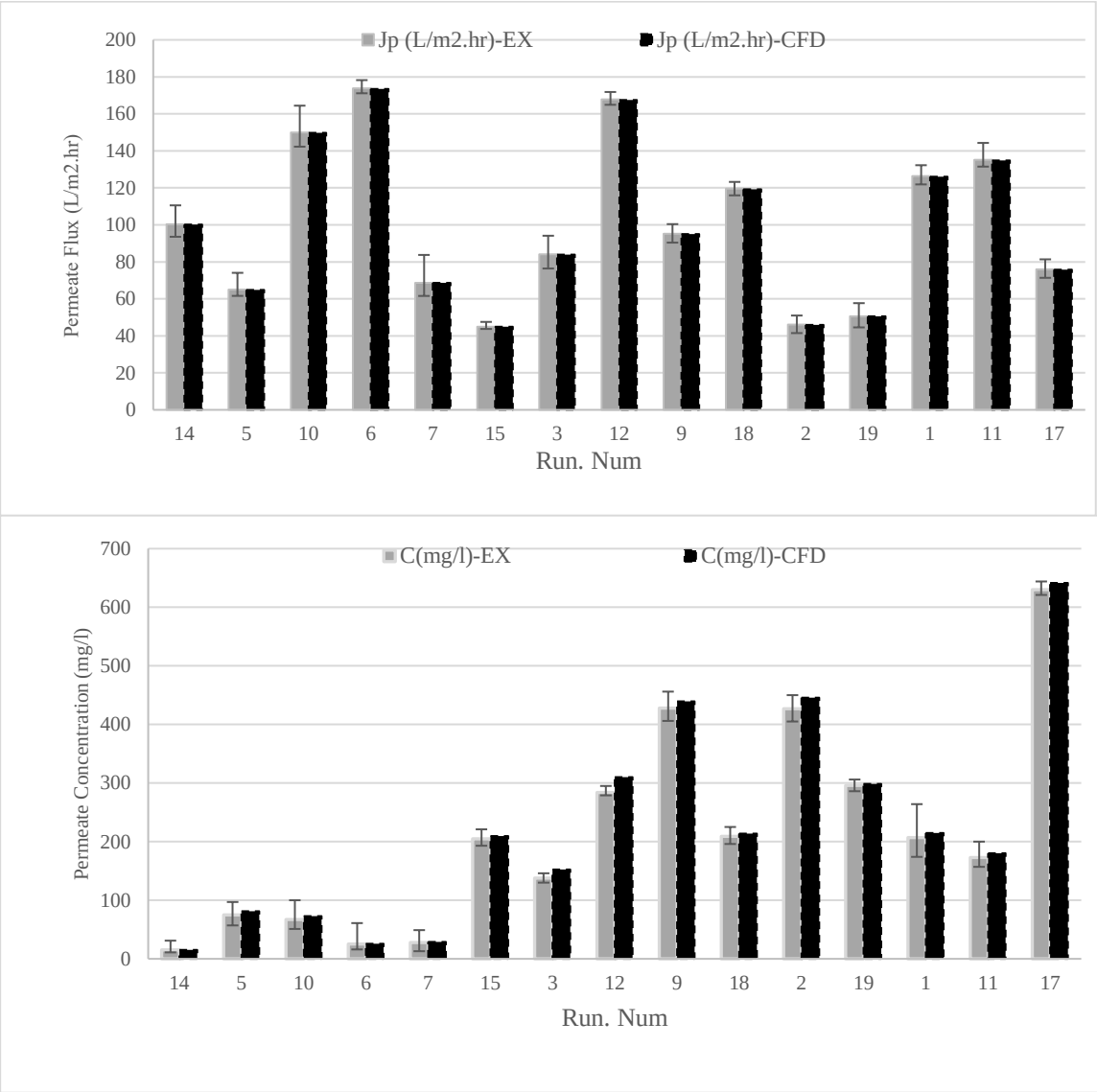

Figure 5. Comparison of CFD and experimental results: (a) permeation flux and (b) permeate concentration in an empty membrane channel.

4.2. Prediction of concentration polarization

Experimental results of the permeate flux show that increasing the feed velocity (0.1, 0.4 and 0.7 m/s) increased the permeate flux (Fig. 5). The reason for this is that an increase in the feed velocity can enhance the shear stress on the membrane surface and reduce the concentration polarization [25,29,37]. Hydrodynamic fluctuations change thickness of the CP layer. In this

work, Reynolds number for laminar flow ($Re_f = \rho u_0 h / \mu$) was 371, 741, 1485, 2220 and 2600.

Fig. 7A shows the flow velocity on the membrane surface and in the middle of the channel (half height=0.0015 m) were minimum and maximum, respectively. Minimum velocity in the vicinity of the membrane surface causes a decline in the momentum force and shear stress which then enhances the CP [28, 38]. Besides, spacer filaments are the reason for the formation of large recirculation regions behind the filaments. Thus, the developing CP layer is repeatedly disturbed by the fluid flow around the filaments and the salt concentration increases before the filaments whereas it decreases on the membrane surface below the filaments because of the flow recirculation in that area (Fig. 7B).

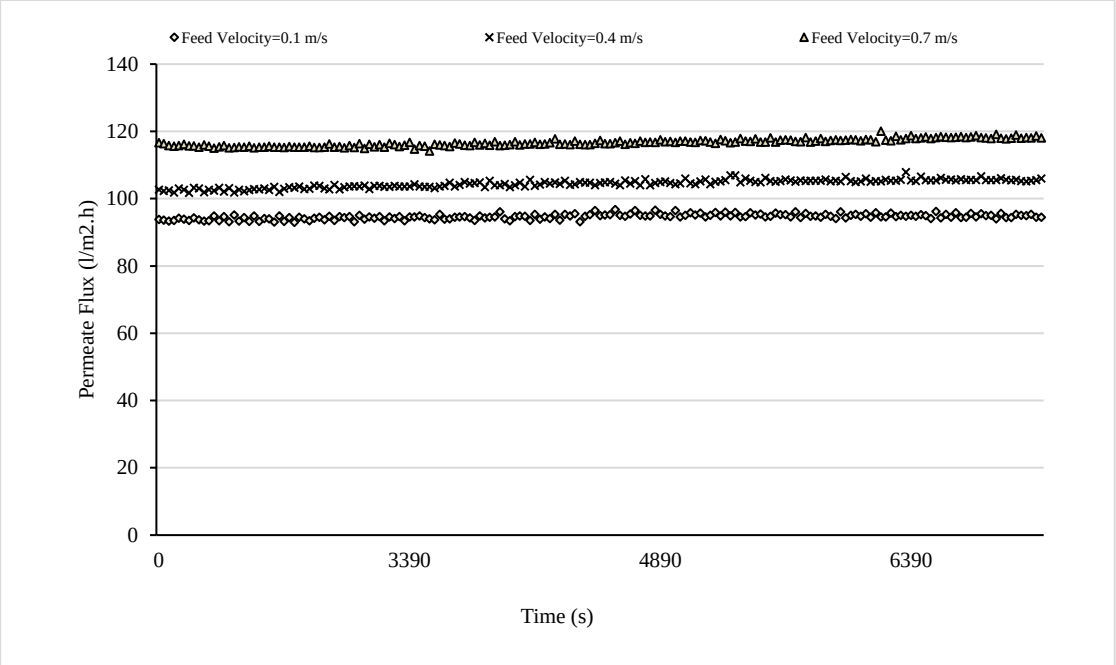

Figure 6. Permeate flux (TMP=9 bar and feed concentration=2500 mg/l).

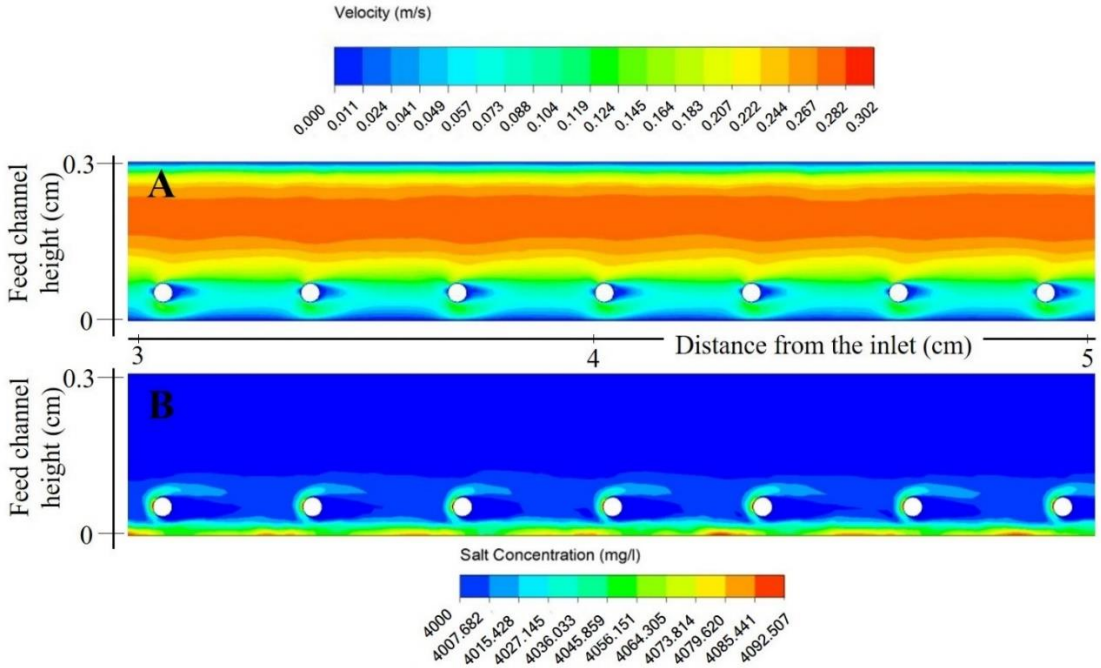

Figure 7. Development of the A) mixture velocity (m/s) and B) concentration polarization (mg/lit) along the membrane surface in the feed channel. Operation conditions: TMP=6 bar, Cf=4000 mg/l, Qfl=2 l/min.

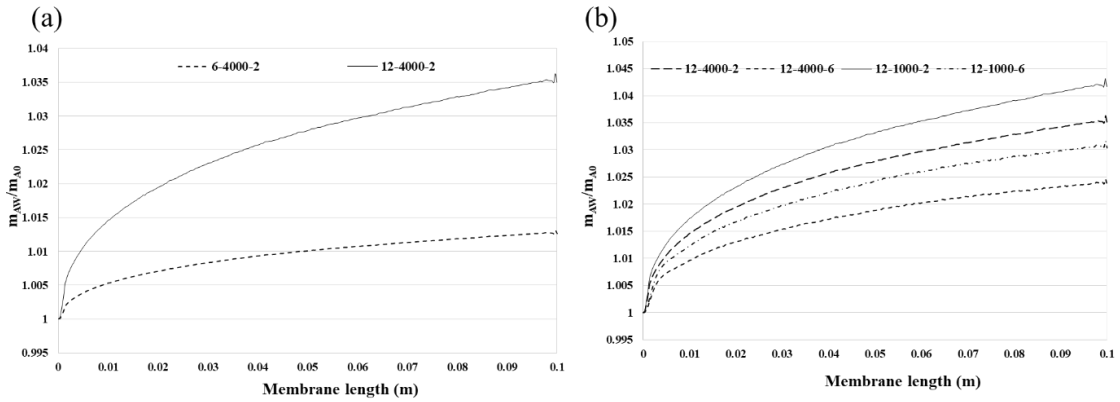

Figure *8*. Fluctuation of concentration in surface membrane adjacent. Operation conditions: (a) effect of TMP, TMP=6, 12 bar, Cf=4000 mg/l, Qf=2 l/min (b) effect of Reynolds number, TMP=12 bar, Cf=4000 and 1000 mg/l, Qf=2 and 6 l/min equal to Re=741 and 2220, respectively.

According to Fig. 8, CP phenomena increased with increasing TMP (Fig. 8a), decreasing the Reynolds number (Fig. 8b) and decreasing the bulk concentration (Fig. 8b). An increase in TMP caused the permeate flux and salt rejection to enhance. Decreasing the Reynolds number (or the feed velocity) made the shear stress lower. At the same TMP and Reynolds number, decreasing in bulk concentration decreased the osmotic pressure and therefore enhanced the permeate flux and salt rejection. It is evident that a rise in bulk concentration leads to increase in peak of the CP profile [39]. Meaning that $m_{AW} - m_{A0}$ in higher bulk concentrations is more than that of lower ones.

$$J_v = L_p(TMP - (\pi_m - \pi_p)) \quad (17)$$

$$\frac{m_{AW}}{m_{A0}} = (1 - R + Rexp\left(-\frac{J_v}{k}\right))^{-1} \quad (18)$$

4.3. Response surface methodology (RSM)

For the experiment design (discussed in section 2.5), the permeate flux varied from 44.875 to 173.75 (L/m^{2}h) and the permeate conductivity ranged from 15 to 428 µs/cm^2. The adequacy of the reduced regression model was considered by the ANOVA and the result of performed tests. To be valid from statistical point of view, the P value (0.0001) should be as low as possible and F value (45.68) must be as high as possible. The noise error chance could occur is 0.01% shown in Table 3.

Table 3. ANOVA tables and statistical parameters

Source	Sum of Squares	Mean of Square	F-value	P-value	
Model	25884.62	2876.07	45.68	< 0.0001	Significant
Residual	566.62	62.96			
Lack of Fit	144.61	28.92	0.27	0.9058	

Fig. 9 depicts the residual normal probability and the residuals versus the predicted response. Fig. 9a shows that the residuals have fallen on a straight line and the errors have been normally distributed. The adequacy of the minimum square fit is also demonstrated. Plots of residuals versus run number and predicted values show a scattering behavior between -3 to +3 (Fig 9b,c). These plots depict that there is no specific pattern and/or unusual structure. Besides, the predicted values versus the actual data has been illustrated with a good agreement of fit in the developed RS model (Fig 9d). Therefore, the model was proved to be adequate to optimize the permeate flux.

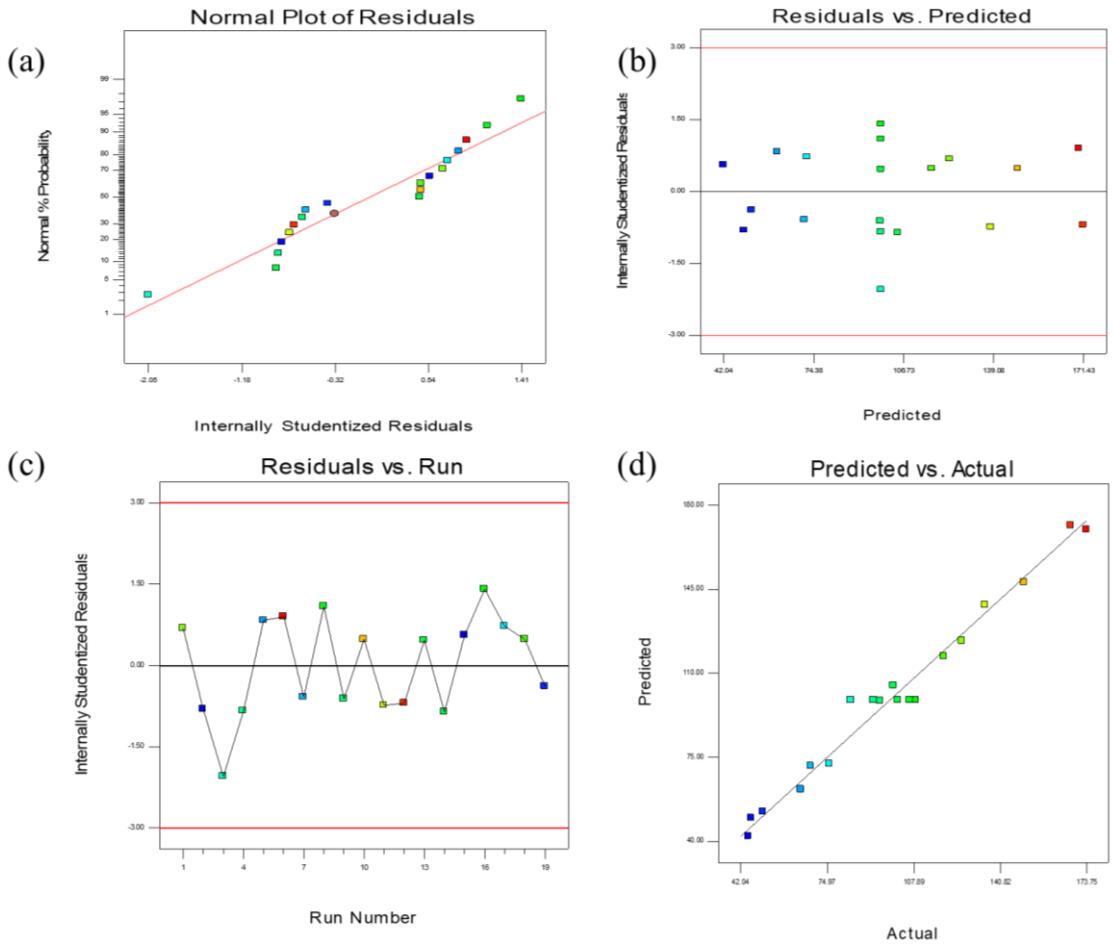

Figure 9.The plots for the CCD design (a, b, c) and the predicted versus actual values (d)

Fig. 10a and 10b indicate that increasing TMP as well as the liquid flow rate increased the permeate flux whereas increasing the feed concentration declined the permeate flux. According to Fig. 10, the effect of TMP in rising CP is more significant than that of the feed flow rate and the feed concentration.

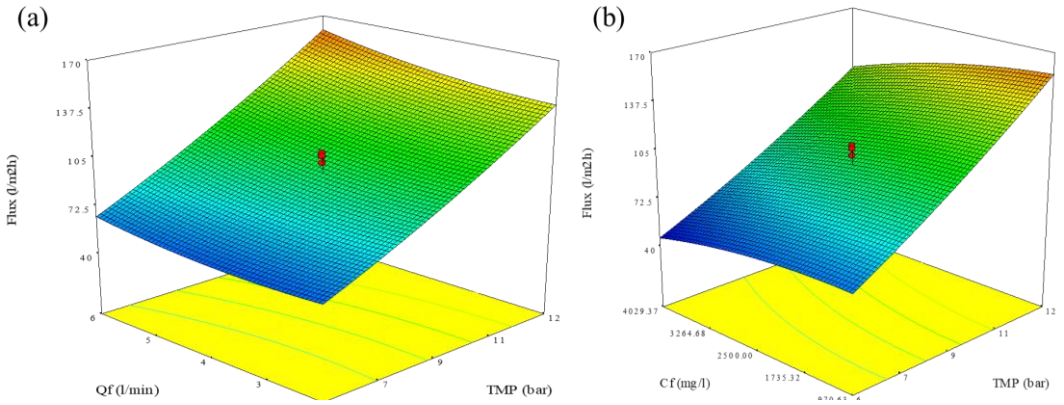

Figure 10.Response surface plot by RSM; predicted permeate flux as a function of feed flow and concentration and TMP (a,b)

4.4. Prediction of concentration polarization by Sherwood correlations

According of the section 3.2, Sherwood number correlation explains the CP phenomena in laminar flows. Eq. (7) is an empirical relations that can calculate the mass transfer coefficient. In this work, the mass transfer coefficient was first calculated using Eq. (5) to (7) and then compared with CFD results. The results of the mass transfer coefficient (k) calculated from Eq. (7) and CFD are shown in Table 4. The results revealed that the mass transfer derived from CFD simulations is more than Sherwood numbers in all experiments. According to mass transfer coefficients indicated for CFD results in Table 4, log ($Sh/SC^{0.33}$) was drawn versus log (Re) (Fig. 11) and then a line regression equation was measured as the Sherwood number (Eq. (19)).

Table 4. Comparison between Sherwood number correlation and CFD values of k.

TMP (bar)	C_f (mg/l)	Q_f (l/min)	$k*10^5$(m/s) (derived from Eqs.(6,7))	$k*10^5$(m/s) (calculated from CFD)
9	250	4	1.23	1.71
6	1000	2	0.978	1.26
12	1000	2	0.978	1.27
12	1000	6	1.41	2.11
6	1000	6	1.41	2.11
4.5	2500	4	1.23	1.66
9	2500	4	1.23	1.71
13.5	2500	4	1.23	1.59
9	2500	1	0.778	0.87
9	2500	7	1.49	2.12
6	4000	2	0.981	1.22
6	4000	6	1.41	2
12	4000	2	0.981	1.3
12	4000	6	1.41	2.07
9	4750	4	1.24	1.57

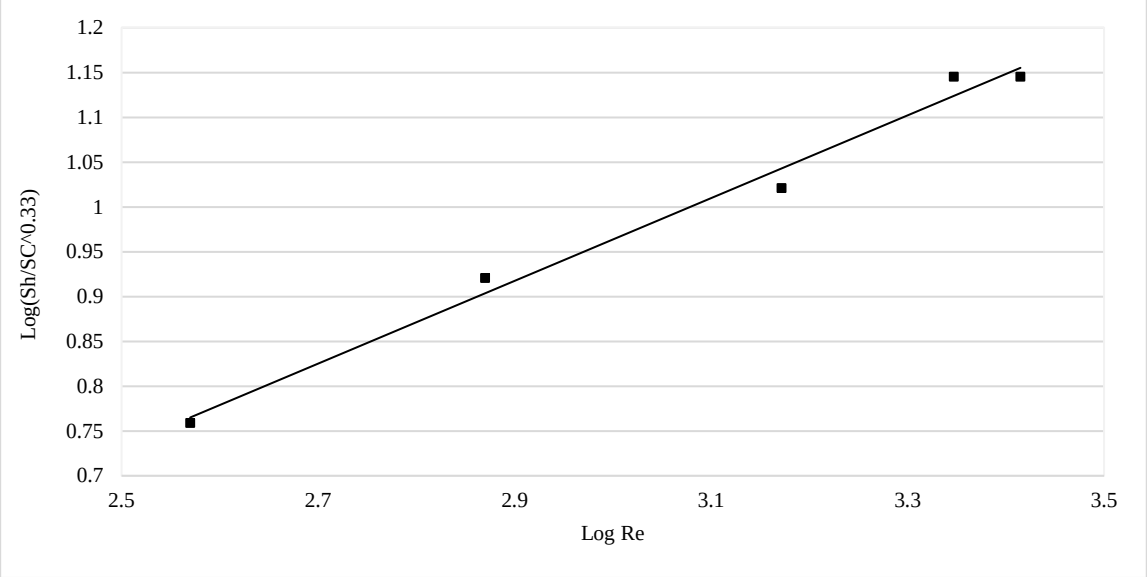

Figure 11.Correlation of the mass transfer data for CFD results.

$$Sh = 1{,}02\, Re^{0{,}461}\left(\frac{Scd_h}{L}\right)^{0{,}33} \quad 19$$

5. Conclusion

In this research, a detailed 2D CFD simulation was conducted to investigate the CP phenomena in nanofiltration of an aqueous solution of $MgSO_4 7H_2O$ in a vertical spacer-filled flat sheet membrane module. Besides, effects of varying the feed concentration, the liquid flow and TMP on the permeate flux and concentration were studied by setting up an RSM statistical analysis. It was shown that the permeate flux was enhanced by either increasing TMP or the liquid flow rate whereas it was reduced by increasing the feed concentration. Finally, the mass transfer coefficient obtained from CFD simulation results and measured from Sherwood empirical relationships were compared showing 10% and 33% tolerance in lower and higher liquid flow rates, respectively. Also, a satisfactory agreement has been achieved when CFD results were compared with the available experimental data.

Nomenclature

c	salt concentration (kg/m^3)
d_h	hydraulic diameter (m)
D	diffusion coefficient (m^2/s)
g	gravitational force (m/s^2)
h	channel height (m)
J_v	permeate volume flux (m/s)
k	mass transfer coefficient (m/s)
L	membrane channel length (m)
L_P	hydraulic conductivity (m^2/(Pa.s))

M	interfacial momentum source term (kg/m^2s^2)
m_A	solute mass fraction (kg solute/kg solution)
m_{Aw}	solute mass fraction on membrane surface (kg solute/kg solution)
p	pressure (Pa)
R	true rejection
TMP	transmembrane pressure (Pa)
u	velocity in x-direction (m/s)
v	velocity in y-direction (m/s)

Greeks letters

α	volume fraction
δ	film layer thickness (m)
μ	viscosity (kg/m s)
ϑ	kinematic viscosity (m^2/s)
π	osmotic pressure (Pa)
ρ	density (kg/m^3)

Subscripts

k	phase k
l	liquid phase
P	permeate side
w	solution adjacent to the wall
0	bulk solution

References

1. Abadikhah H., Zokaee Ashtiani F., Fouladitajar A., (2015). Nanofiltration of oily wastewater containing salt; experimental studies and optimization using response surface methodology, Desalin. Water Treat. 56:2783–2796.
2. Mulder M., Basic principles of membrane technology, Kluwer Academic, 1991.
3. Zeng K., Zhou J., Cui Z., Zhou Y., Shi C., Wang X., Zhou L., Ding X., Wang Z., Drioli E., (2018). Insight into fouling behavior of poly(vinylidene fluoride) (PVDF) hollow fiber membranes caused by dextran with different pore size distributions, Chinese J. Chem. Eng. 26: 268–277.
4. Geraldes V., Afonso M.D., (2007). Prediction of the concentration polarization in the nanofiltration/reverse osmosis of dilute multi-ionic solutions, J. Memb. Sci. 300: 20–27.
5. Prabhavathy C., De S., (2010). Estimation of transport parameters during ultrafiltration of pickling effluent from a tannery, Sep. Sci. Technol. 45:11–20.
6. Mercier-bonin M., Daubert I., Le D., Maranges C., Fonade C., Lafforgue C., (2001). How unsteady filtration conditions can improve the process efficiency during cell cultures in membrane bioreactors, Sep. Purif. Technol. 22–23: 601–615.
7. Liikanen R., Yli-Kuivila J., Laukkanen R., (2002). Efficiency of various chemical cleanings for nanofiltration membrane fouled by conventionally-treated surface water, J. Memb. Sci. 195:265–276.
8. Asefi H., Alighardashi A., Fazeli M., Fouladitajar A., (2019). CFD modeling and simulation of concentration polarization reduction by gas sparging cross-flow nanofiltration, J. Environ. Chem. Eng.7 : 103275, 1-7.

9. Asadi Tashvigh A., Zokaee Ashtiani F., Fouladitajar A., (2016). Genetic programming for modeling and optimization of gas sparging assisted microfiltration of oil-in-water emulsion, Desalin. Water Treat. 57 : 19160–19170.
10. Cui Z.F., Wright K.I.T., (1996). Flux enhancements with gas sparging in downwards crossflow ultrafiltration: Performance and mechanism, J. Memb. Sci. 117 : 109–116.
11. Jaffrin M.Y., (2008). Dynamic shear-enhanced membrane filtration: A review of rotating disks, rotating membranes and vibrating systems, J. Memb. Sci. 324 : 7–25.
12. Sarkara B., Deb S., (2010). Electric field enhanced gel controlled cross-flow ultrafiltration under turbulent flow conditions, Sep. Purif. Technol. 74 :73–82.
13. Ducom G., Puech F.P., Cabassud C., (2002). Air sparging with flat sheet nanofiltration: A link between wall shear stresses and flux enhancement, Desalination. 145 : 97–102.
14. Ahmed S., Seraji M.T., Jahedi J., Hashib M.A., (2012) . Application of CFD for simulation of a baffled tubular membrane, Chem. Eng. Res. Des. 90:600–608.
15. Schock A.M. G., (1987) Mass transfer and pressure loss in spiral wound modules, Desalination. 64 : 339 – 352.
16. B. hallstrom Vassilis gekas, (1987). Mass transffer in the membrane concentration polarization layer under turbulent cross flow, J. Memb. Sci. 30 : 153.
17. Li M., Bui T., Chao S., (2016) Three-dimensional CFD analysis of hydrodynamics and concentration polarization in an industrial RO feed channel, Desalination. 397 :194–204.
18. Fouladitajar A., Zokaee Ashtiani F., Rezaei H., Haghmoradi A., Kargari A., (2014). Gas sparging to enhance permeate flux and reduce fouling resistances in cross flow microfiltration, J. Ind. Eng. Chem. 20 : 624–632.
19. Shakaib M., Hasani S.M.F., Mahmood M., (2009) . CFD modeling for flow and mass transfer in spacer-obstructed membrane feed channels, J. Memb. Sci. 326 :270–284.
20. Monfared M.A., Kasiri N., Salahi A., Mohammadi T., (2012). CFD simulation of baffles arrangement for gelatin-water ultrafiltration in rectangular channel, Desalination. 284 : 288–296.
21. Ahmed S., Taif Seraji M., Jahedi J., Hashib M.A., (2011). CFD simulation of turbulence promoters in a tubular membrane channel, Desalination. 276 : 191–198.
22. Wardeh S., Morvan H., (2008). CFD simulations of flow and concentration polarization in spacer-filled channels for application to water desalination, Chem. Eng. Res. Des. 86 : 1107–1116.
23. Sutzkover I., Hasson D., Semiat R., (2009). Simple technique for measuring the concentration polarization level in a reverse osmosis system, 131 : 117–127.
24. Geraldes V., Afonso M.D., (2006). Generalized mass-transfer correction factor for nanofiltration and reverse osmosis, AIChE J. 52 : 3353–3362.
25. Fernandez-Sempere J., Ruiz-Bevia F., Garcia-Algado P., Salcedo-Diaz R., (2010). Experimental study of concentration polarization in a crossflow reverse osmosis system using Digital Holographic Interferometry, Desalination. 257: 36–45.
26. Subramani A., Kim S., V Hoek E.M., (2006). Pressure, flow, and concentration profiles in open and spacer-filled membrane channels, J. Memb. Sci. 277 : 7–17.
27. Geraldes V., Semiao V., De Pinho M.N., (2004). Concentration polarisation and flow structure within nanofiltration spiral-wound modules with ladder-type spacers, Comput. Struct. 82 : 1561–1568.
28. Salcedo-Díaz R., García-Algado P., García-Rodríguez M., Fernández-Sempere J., Ruiz-Beviá F., (2014). Visualization and modeling of the polarization layer in crossflow reverse osmosis in a slit-type channel, J. Memb. Sci. 456 : 21–30.

29. Ahmad A.L., Lau K.K., (2006). Impact of different spacer filaments geometries on 2D unsteady hydrodynamics and concentration polarization in spiral wound membrane channel, J. Memb. Sci. 286 : 77–92.
30. Kim S., V Hoek E.M., (2005). Modeling concentration polarization in reverse osmosis processes, Desalination. 186 : 111–128.
31. Baker R.W.,(2004). Membrane Technology and Applications, John Wiley & Sons, Ltd, Chichester, UK.
32. Khayet M., Seman M.N.A., N. Hilal, (2010). Response surface modeling and optimization of composite nanofiltration modified membranes, J. Memb. Sci. 349.
33. Khayet C.C. M., Essalhi M., (2011). Artificial neural network modeling and response surface methodology of desalination by reverse osmosis, J. Memb. Sci. 368 : 13.
34. Li R.G. Q.Y., Bellara S.R. , Cui Z.F. , Pepper D.S., (1998). Enhancement of ultrafiltration by gas sparging with flat sheet membrane modules, Sep. Purif. Technol. 14: 5.
35. Ishii M., Thermo-fluid dynamic theory of two-phase flow, Eyrolles, Paris, 1975
36. Issa R.I., (1986). Solution of the Implicit Discretized Fluid Flow Equations by Operator Splitting, J. Comput. Phys. 62 : 40–65.
37. Cavaco Morão A.I., Brites Alves A.M., Geraldes V., (2008). Concentration polarization in a reverse osmosis/nanofiltration plate-and-frame membrane module, J. Memb. Sci. 325: 580–591.
38. Karode S.K., Kumar A., (2001). Flow visualization through spacer filled channels by computational fluid dynamics I. Pressure drop and shear rate calculations for flat sheet geometry, J. Memb. Sci. 193 : 69–84.
39. Zare M., Fouladitajar A.,(2013). CFD modeling and simulation of concentration polarization in microfiltration of oil–water emulsions; Application of an Eulerian multiphase model, Desalination. 324:11.